Emmanuel O. Okechukwu, 2025, 13:6 ISSN (Online): 2348-4098 ISSN (Print): 2395-4752

An Open Access Journal

# Investigating the Doping Effects on the Optical, Electrical, Structural, Morphological, Elemental Composition, and Magnetic Properties of Electrodeposited TI-Doped Cus Thin Films

Emmanuel O. Okechukwu.<sup>a\*</sup>, Azubuike J. Ekpunobi,<sup>a</sup> Azubogu, A. C. O.,<sup>b</sup> Onuigbo, E. N.,<sup>c</sup> Overcomer Anusiuba,<sup>d</sup> Adline Nwodo,<sup>e</sup> Diemiruaye M. Jeroh,<sup>a</sup> Chukwudi B. Muomeliri,<sup>a</sup> Chiedozie Okafor,<sup>a</sup> Lynda A. Ozobialu,<sup>a</sup> Chiamaka Onu,<sup>a</sup> Uche E. Ekpunobi,<sup>f</sup> Nonso L. Okoli,<sup>g</sup> Ogbodo, E. U,<sup>b,h</sup>

<sup>a</sup>Department of Physics and Industrial Physics, Nnamdi Azikiwe University, Awka
<sup>b</sup>Department of Electronics and Computer Engineering, Nnamdi Azikiwe University, Awka
<sup>c</sup>Department of Geological Sciences, Nnamdi Azikiwe University, Awka
<sup>d</sup>Department of Computer Science, Nnamdi Azikiwe University, Awka
<sup>e</sup>Magnetism and Magnetoscience Laboratory, Kagoshima University, Japan
<sup>f</sup> Department of Pure and Industrial Chemistry, Nnamdi Azikiwe University, Awka
<sup>g</sup>Nanoscience and Advanced Materials, Federal University of ABC, Santo Andre, Sao Paulo, Brazil
<sup>h</sup>Department of Electrical Engineering, Tshwane University of Technology, South Africa

Abstract- Successfully, thin films of copper (II) sulfide (CuS) and titanium-doped copper (II) sulfide (Ti:CuS) have been deposited on fluorine tin-doped oxide (FTO) glass substrates, using electrodeposition technique, at room temperature. The films were characterized to investigate their optical, structural, morphological, compositional, electrical, and magnetic properties, using UV-Vis spectrophotometer (at wavelength range of 300 nm – 1100 nm), x-ray diffractometer machine, scanning electron microscope equipped with energy dispersive x-ray spectroscope, four-point probe technique, and vibrating sample magnetometer (VSM), respectively. Thickness of the films was obtained using a profilometer, and thickness values of 109.16 nm, 113.17 nm, 121.11 nm, and 131.79 nm were obtained for the undoped CuS thin film, 2 % Ti doped, 6 % Ti doped, and 10 % Ti doped thin films, respectively. Optical bandgap of the films range between 2.40 eV and 2.60 eV. Structural analysis of the films confirmed hexagonal phase of CuS with lattice constant, a=b=3.7920 Å and c=16.3440 Å.

Keywords- DMS; electrodeposition; Ti doping; bandgap; UV-VIS spectroscopy; XRD; SEM-EDS; four-point probe; VSM

## I. INTRODUCTION

In search of materials with special properties, for more advanced technological applications, synthesis and characterization of dilute magnetic semiconductors (DMSs) films have gained tremendous research interest, in recent years. Most recently researched on, are the thin films of copper (II) sulfide doped with titanium ion, because of their unique spintronic properties. Dilute magnetic semiconductors are materials that combine the properties of both semiconductors and magnetic materials [1]. They are typically created by introducing a small amount of magnetic elements, such as transition metals, into a semiconductor crystal lattice, without changing the lattice that

© 2025 Emmanuel O. Okechukwu. This is an Open Access article distributed under the terms of the Creative Commons Attribution License (http://creativecommons.org/licenses/by/4.0), which permits unrestricted use, distribution, and reproduction in any medium, provided the original work is properly credited.

emerged from the resulting materials, for lots of modern devices [2]. This doping introduces a localized magnetic moments that can interact with the electron spin in the semiconductor. Dilute magnetic semiconductors have their promising applications in spintronics [3-5], where electron spin is utilized for information storage and processing [6], quantum bits for quantum computation and communication [7], nanoscale integrated magnetic memories and sensors [8], data storage [9], magneto-optoelectronic devices [10],

Among different metal chalcogenides, copper sulfide has been extensively studied and has attracted much interest in the recent research due to its special properties and potential applications such as in solar cells [11], cathode material in lithium chargeable batteries [12], optical data storage [13], fabrication of microelectronic devices, optical filters as well as in low temperature gas sensor applications [14], gas sensors [15], photochemical conversion of solar energy as solar absorber coating and photoconductive coatings [16].

Thin films of copper sulfide have been grown using various techniques, which include chemical bath deposition (CBD) [17], chemical spray pyrolysis (CSP) [18, 19], atomic layer deposition (ALD) [20], electrodeposition [21], and pulsed laser deposition (PLD) technique [22]. Among them all, electrodeposition has been considered the best deposition technique, because of its advantages such as: low cost effective, simplicity, high growth rate at relatively low temperature, and easier control of film thickness, morphology, and composition [23-26].

Our present work gears towards doping copper (II) sulfide (CuS) thin films with titanium (Ti) impurities, so as to investigate their unique properties, for possible technological applications, using the simple and low-cost electrodeposition technique.

# II. EXPERIMENTAL PROCEDURE: MATERIALS AND METHOD

Three-electrode cell set-up was adopted in the films' deposition, where we used the FTO as the working electrode, silver – silver chloride electrode (Ag/AgCl) as reference electrode, and platinum wire as a counter electrode. The glass substrates were ultrasonically cleaned in ethanol for 30 minutes (at 30 °C), rinsed with distilled water, and allowed to dry before use.

## 1. Deposition of Undoped Copper (II) Sulphide (CuS) Thin Film

The bath solution for the deposition of CuS thin films contained 15 ml of 0.05 molar concentration of copper (ii) sulphate pentahydrate (CuSO4.5H2O) as a source of copper ion (Cu2+) and 15 ml of 0.05 molar concentration of thiourea (CH4N2S) as a source of sulfur ion (S2-). The solution was mixed properly using a magnetic stirrer. The 0.05 M of CuSO4.5H2O was prepared by dissolving 6.2 g of it in 500 ml of distilled water; and the 0.05 M of CH4N2S was prepared by dissolving 1.9 g of it 500 ml of distilled water. The film deposition took place at room temperature of 27 °C. The pH value (2.9) of the bath solution was obtained using a pH meter. The deposition time and voltage were kept at 10 s and 5 V respectively, as shown in Table 1. After deposition, the sample was taken out of the solution carefully, and immersed in distilled water for just two seconds, and then allowed to dry in flowing air. Afterwards, the sample was placed in a slide box, labelled accordingly.

Sample

Conc.(M)

Vol.(ml)

Vol.(ml)

PH

Temperature
(°C)

Voltage
(N)

Time
(s)

Cu S	0.05	15	0.05	15	2.5	27	2	10	
---------	------	----	------	----	-----	----	---	----	--

# 2. Deposition Of Ti-doped Copper (II) Sulphide (Ti :CuS) Thin Films

The combination of ionic concentrations for doping of CuS with titanium is given in Table 2. By varying the relative ratio of Cu and Ti ions, the  $Cu_{1-x}Ti_xS$  films with solution parameter x=0.00, 0.02, 0.06, and 0.10 were deposited. The percentage doping was varied from 2% - 10% at an interval of 4%.

Table 2: Doping formulations of precursors used for deposition of  $Cu_{1-x}Ti_xS$ 

$acposition of cu_{1-x} r_{x} s$								
Composition parameter (x)	Percentage doping (%)	Concentration of copper sulphate (mole)	Concentration of titanium chloride (mole)	Concentration of thiourea (mole)				
0.00	0	0.050	0.000	0.050				
0.02	2	0.049	0.001	0.050				
0.06	6	0.047	0.003	0.050				
0.10	10	0.045	0.005	0.050				

During deposition, pH of the solution bath was kept at a constant value of 2.2, using ammonia solution (NH3), and the films' deposition took place at room temperature of 27 oC, voltage value of 5 V, and time of 10 s, as given in Table 3.

Table 3: Variation of percentage doping for the deposition of <code>[Cu]</code> \_(1-x) <code>[Ti]</code> \_x S Thin Films

Sample	$CuSO_4.5H_2O$		$TiCl_3$		$CH_4N_2S$		$NH_3$	Hd	Temp.	Doping	Voltage	i
	Со	Vol	Co	lo/	Co	Vol	Co		_		>	
CuS	0.050	15	0.000	10	050'0	15	0.05					

Ti:2%	0.049	15	0.001	10	0:020	15	0.050	2.2	27	2	2	7
%9:I1	0.047	15	0.003	10	0.050	15	0:020	2.2	27	9	2	0
Ti:10%	0.045	15	0.005	10	0:020	15	0.050	2.2	27	10	2	7

### 3. Film Charactrization

The deposited films were characterized in order to investigate their optical, electrical, structural, morphological, compositional, and magnetic properties. The optical characterization was done using a UV-VIS spectrophotometer (model: 756S UV-VIS) to obtain the optical absorption data of the films, within the wavelength range of 300 nm -1100 nm. Four-point probe technique (Keithley 2400 - LV source meter) was employed to analyse the electrical properties of the films. The films structural properties were studied using an X-ray diffractometer (Bruker D8 high-resolution diffractometer) using Cu K $\alpha$  line ( $\lambda$  = 1.54056 Å). Surface morphology and elemental composition of the films were also studied using Nova NanoSEM and MIRA TESCAN SEM machine. The magnetic properties of the films were obtained using vibrating sample magnetometer (Model: EZ 10 by MicroSense), while the films thicknesses were measured with the aid of a profilometer (Model: Veeko Dektak 150).

#### III. RESULTS AND DISCUSSION

# 1. Effect of titanium concentration on the thickness of CuS thin films

Figure 4.1 depicts the effect of titanium concentration on the thickness of CuS thin films.

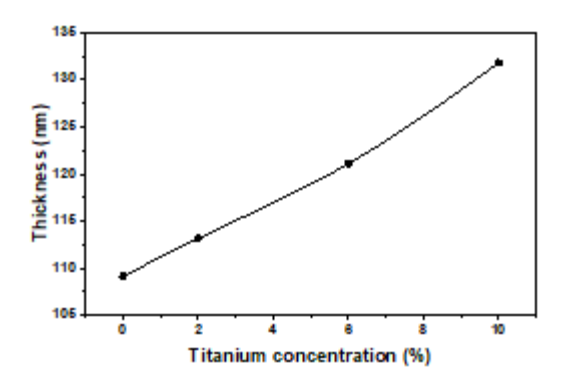


Figure 1: Effect of titanium concentration on the thickness of CuS thin films

The figure revealed a linear increase in the thickness of the films (from 109.16 nm to 131.79 nm) as titanium concentration was increased from 2 % to 10%.

## 2. Optical Analysis

From the measured absorbance data of the undoped and titanium-doped copper (II) sulfide thin films, the optical properties of the films, such as the transmittance (T), the reflectance (R), the refractive index, extinction coefficient, optical conductivity, energy band gap, real and imaginary dielectric constants, were evaluated using the appropriate equations. The transmittance (T) of the deposited films was evaluated using  $T=10^{-A}$  [28, 29], where A is the absorbance. While R = 1- (A + T) as given by [30, 31], was used to evaluate the reflectance (R) of the deposited films.

## Absorbance (A), Transmittance (T), and Reflectance (R) Plots

Plots of the absorbance, transmittance, and reflectance of the deposited films of undoped copper (II) sulfide (CuS) and titanium-doped copper (II) sulfide (Ti:CuS) are depicted in Figure 4 (a-c).

The optical absorption coefficient ( $\alpha$ ) of the films was calculated using equation (5), as given by [32-34]:

$$\alpha = \frac{1}{t} \ln \left( \frac{1}{T} \right) \tag{5}$$

Where t is the thickness of the films and T is the transmittance. The extinction coefficient (K) of the

deposited films was evaluated using equation (6), as given by [35, 36]:

$$k = \frac{\alpha \lambda}{4\pi}$$
 (6)

The refractive indices of the samples were calculated using equation (7), as given by [37, 38]:

$$\eta = \frac{1+R}{1-R} + \sqrt{\frac{4R}{(1-R)^2} - k^2} \tag{7}$$

The optical conductivity ( $\sigma_o$ ) of the films was calculated using equation (8), as given by [39, 40]:

$$\sigma_o = \frac{\alpha \eta c}{4\pi} \tag{8}$$

where c is the speed of light. The energy band gap of the films was calculated using Tauc's formula for near-band edge absorption, as given by [41 - 44]:

$$(\alpha h v)^n = A(h v - E_a) \tag{9}$$

where  $\alpha$  is the optical absorption coefficient, A is the transition probability constant, h is the Planck's constant, v is the frequency of incident radiation,  $E_g$  is the band gap of the films and n is the characteristic constant for the optical transition. The optical band gap energy  $(E_g)$  of our deposited films were obtained by extrapolating the straight portion of the plot of  $(\alpha hv)^2$  against the photon energy (hv) at  $(\alpha hv)^2 = 0$ . The films' complex dielectric function was estimated from the relation given by [45, 46]:

$$\mathcal{E} = \mathcal{E}_r + \mathrm{i}\mathcal{E}_i \qquad (10)$$

$$\mathcal{E}_r = n^2 - k^2 \quad (11)$$

$$\mathcal{E}_i = 2nk \tag{12}$$

Where  $\mathcal{E}_r$  and  $\mathcal{E}_i$  are the real and imaginary parts of the dielectric constant, respectively. Figures (4.2), (4.3), and (4.4) show the absorption spectral, transmittance, and reflectance of the undoped CuS and Ti-doped CuS thin films, respectively.

From Figure 4.2, the absorbance spectra showed a uniform decrease in absorbance as photon wavelength increased across UV and VIS regions,

with a very slight increase within the NIR region. Also, absorbance was found to have increased as percentage of titanium increased. The increase in absorption of photon energy is an evidence that there is substitution of copper ions by titanium ions in the lattice structure of copper sulfide. Figure 4.3 revealed that the transmittance values of the films increased uniformly with increase in wavelength within UV and VIS regions, but showed a slight decrease at NIR region. This high transmission indicates the high level of homogeneity of the films. Also, transmission of the films were found to decrease as the dopant concentration was increased. Reflectance of the thin films increased within UV region, as wavelength increased, with the exception of the undoped and 2 % Ti doped copper sulfide thin films that started decreasing from the UV region, as shown in Figure 4.4. From the results obtained, Ti-doped CuS films recorded low reflection compared to the undoped CuS films. This could be attributed to the high absorbance nature of the films, caused by the thickness, which increased as the titanium percentage concentration was increased. The results showed that these films are good absorber of photon energy within the visible region and could be used to shed UV radiation and for antireflective coatings.

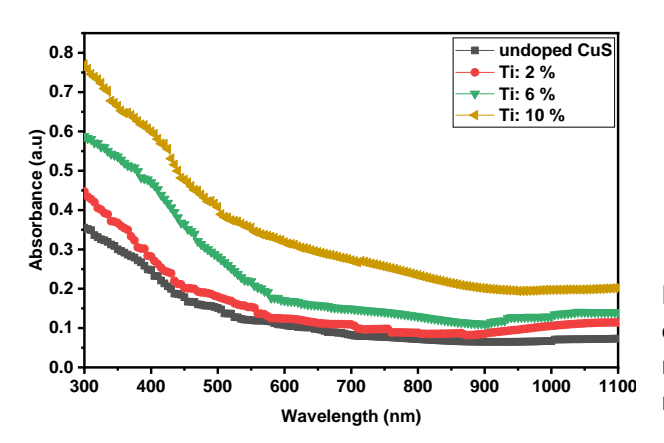


Figure 2: Plot of absorbance against wavelength for undoped and titanium-doped copper (II) sulfide thin films deposited at different titanium concentrations

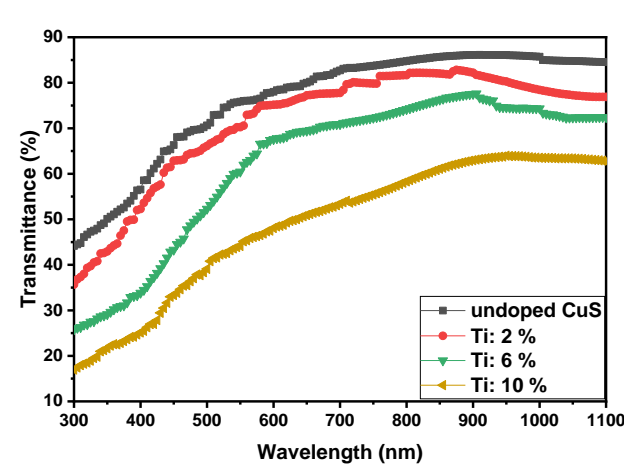


Figure 3: Plot of transmittance against wavelength for undoped and titanium-doped copper (II) sulfide thin films deposited at different titanium concentrations

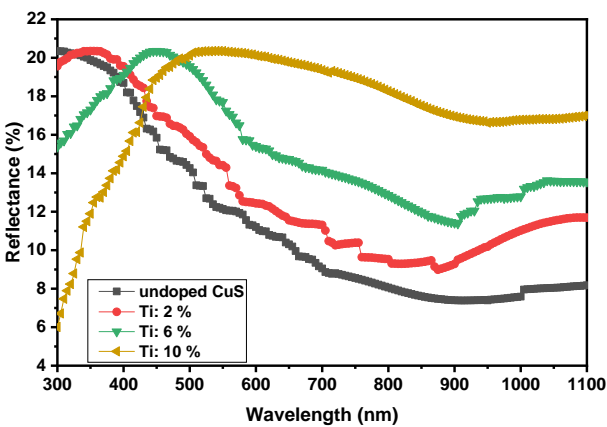


Figure 4: Plot of reflectance against wavelength for undoped and titanium-doped copper (II) sulfide thin films deposited at different titanium concentrations

Figures 5 – 4.9 show the plots of extinction coefficient, refractive index, optical conductivity, real, and imaginary dielectric constants of the films, respectively.

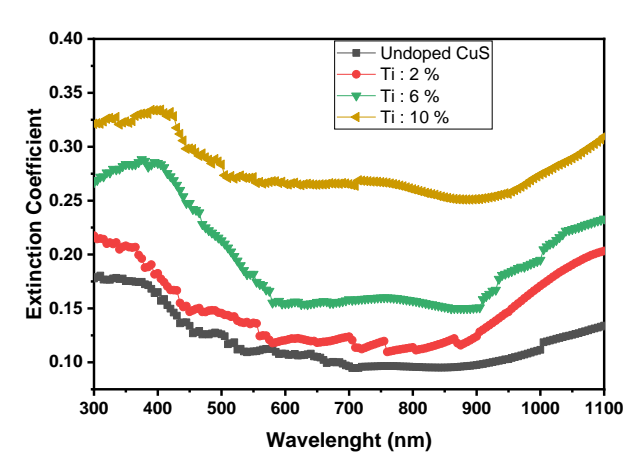


Figure 5: Plot of extinction coefficient against wavelength for undoped and titanium-doped copper (II) sulfide thin films deposited at different titanium concentrations

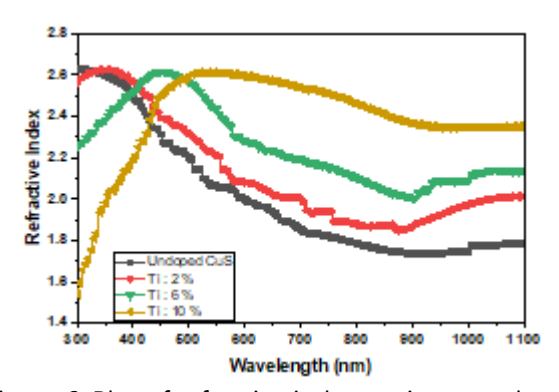


Figure 6: Plot of refractive index against wavelength for undoped and titanium-doped copper sulfide (II) thin films deposited at different titanium concentrations

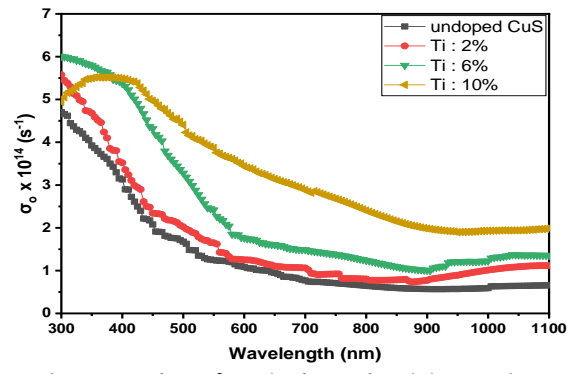


Figure 7: Plot of optical conductivity against wavelength for undoped and titanium-doped copper (II) sulfide thin films deposited at different titanium concentrations

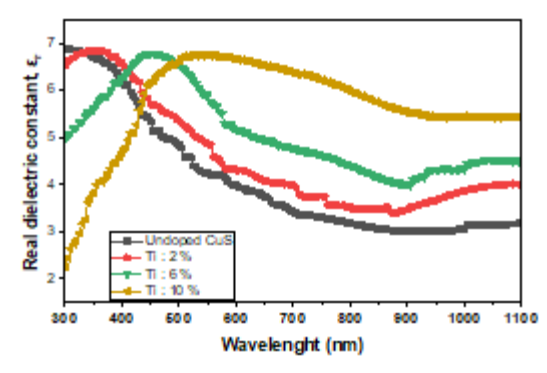


Figure 8: Plot of real dielectric constant against wavelength for undoped and titanium-doped copper (II) sulfide thin films deposited at different titanium concentrations

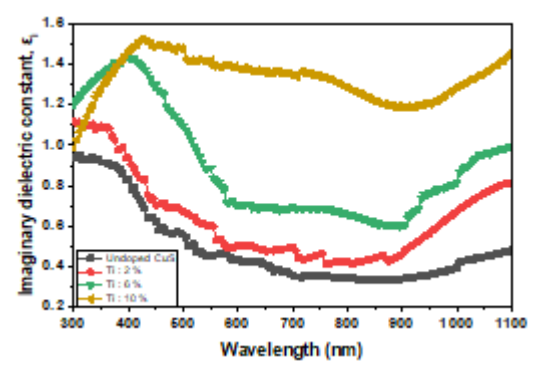


Figure 9: Plot of imaginary dielectric constant against wavelength for undoped and titanium-doped copper (II) sulfide thin films deposited at different titanium concentrations

The graph (Fig. 4.5) revealed that the extinction coefficient of undoped CuS films decreased within UV-VIS (300 nm - 700 nm) regions, and increased at NIR region (800 nm), while Ti-doped CuS films decreased as wavelength increased from 300 nm -560 nm, then remained steady before increasing at 880 nm. From Fig. 4.6, the result obtained showed that refractive index of the films was reducing (at 300 nm), as doping percentage concentration was increased. The result shown in Fig. 4.7 is a revelation of the fact that, as Ti doping concentration was increased from 2 % to 6 %, the optical conductivity values increased, and then decreased beyond 6 % doping concentration (at 300 nm). Also, the Figure showed that optical conductivity of the deposited thin films decreased with increased wavelength. From Fig. 4.8, it can be observed that the undoped CuS thin film recorded

the highest real dielectric constant within UV region. But with the introduction of titanium ion as a doping agent, the real dielectric constant decreased within the UV region. Furthermore, within the VIS region, real dielectric constant increased with doping concentration. The graph (Fig. 4.9) showed that the imaginary dielectric constant of the films decreased (from 350 nm) within UV – VIS region, but increased within NIR region. Also, the results obtained across the wavelengths showed that imaginary dielectric constant values increased with the doping concentration.

Figure 4.10 is the plot of  $(\alpha hv)^2$  against photon energy for undoped and titanium-doped copper (II) sulfide thin films. From the graph, energy band gap of the films were estimated by extrapolation of the straight portion of the graph along the photon energy axis where  $(\alpha hv)^2=0$ . Energy band gap of 2.40 eV, 2.60 eV, 2.40 eV, and 2.55 eV, were recorded for the undoped CuS thin film, 2 %, 6 %, and 10 % titanium-doped CuS thin films, respectively.

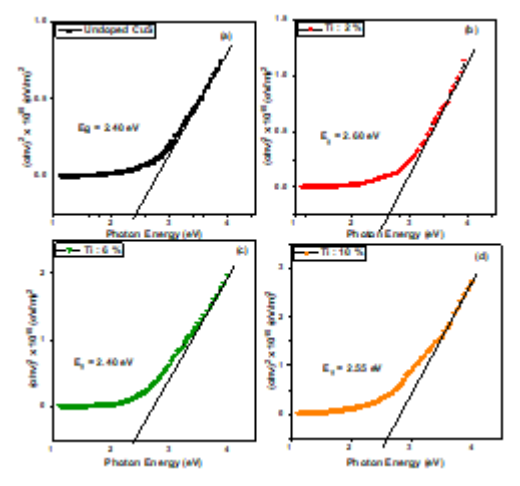


Figure 10: Plot of (αhv)2 against photon energy for undoped and titanium-doped copper (II) sulfide thin films deposited at different titanium concentrations

As it is shown in the figure, the introduction of titanium dopant (2 %) into the precursor of copper sulfide thin film, altered the energy bandgap of the deposited CuS film. This is based on the fact stated

by [47], that titanium doping can increase the carrier concentrations and shift the Fermi level towards the conduction band that leads to shift in absorption edge towards the higher energies. However, at 6 % doping, the energy bandgap droped to a value similar to the undoped CuS film (2.40 eV), which could be as a result of the possibility of formation of some related titanium phases such as TiS, with the same energy bandgap as the undoped CuS film. The energy bandgap increased further with higher percentage doping (10 %).

## 3. Structural Analysis

Fig. 4.11 reveals the XRD pattern of the films, which was used to analyze the structural behavior of the electrodeposited thin films.

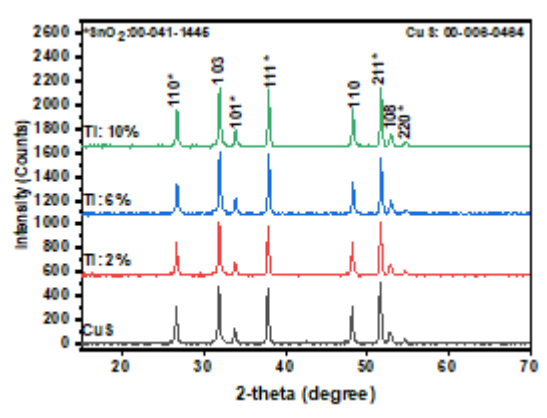


Figure 11 (a): Structural patterns of undoped and Ti-doped copper (II) sulfide thin films

The matching of the calculated d<sub>hkl</sub> values and the standard ones confirms that all the deposited films crystallize well in the hexagonal structure with preferential orientation of the crystallites along the (103) direction with 2 theta angles of 31.813 °, 31.841 °, 31.919 °, and 31.910 ° for the undoped and titanium-doped copper sulfide thin films, respectively, and lattice constant a<sub>-</sub>b<sub>-</sub> 3.7920 Å and c = 16.3440 Å. Increase in dopant concentration caused an increase in intensity of the diffraction peaks and shift in the peaks towards larger angles as can be observed in Table 4.7. Peak shift towards higher angles as titanium ion concentration was increased could be due to the fact that titanium ions simply occupied copper ions' sites. This substitutional occupation of copper ion sites by titanium ions, caused peak shift towards higher angles due to expansion of the lattice constant of the host ion (Cu<sup>2+</sup>). The average crystal sizes (range from 27.761 nm to 31.455 nm) shown in Table 4.3 were calculated using Debye-Scherrer's relation [48, 49] given as:

 $D = \frac{k \lambda}{\beta \cos \theta} \quad (13)$ 

Where k=0.9 (the shape factor);  $\lambda=X$ -ray wavelength;  $\beta=Full$  Width Half Maximum; and D= grain size.

From the values of the crystallite size obtained, the dislocation density ( $\delta$ ), the microstrain ( $\epsilon$ ) and the inter-planer spacing (d) [50] of the deposited films, were calculated using equations (14), (15) and (16), respectively:

$$\delta = \frac{1}{D^2} \tag{14}$$

$$\varepsilon = \frac{\beta}{4 \tan \theta} \quad (15)$$

$$d = \frac{\lambda}{2\sin\theta} \quad (16)$$

The XRD results obtained showed that, with the increase in dopant percentage, crystallite size of the films increased, while dislocation density and micro-strain decreased. This could be attributed to improvement in the crystal structure due to titanium ion doping. Figure 4.11 (b) shows the variation of crystallite size and dislocation density with concentration of dopant ion (titanium ion).

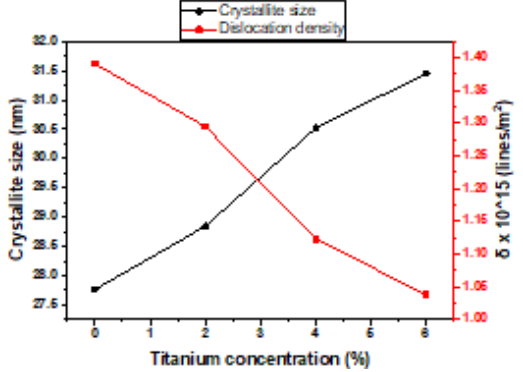


Figure 11 (b): Variation of crystallite size and dislocation density with titanium ion concentration

for undoped and titanium-doped copper sulfide (II) thin films

Table 3: Structural parameters of Ti-doped copper (II) sulfide thin films at varied concentrations of titanium ions

	1		titaniui	11 10115			
	2 0 (°)	hkl	d – spacing (nm)	FWHM (°)	D (nm)	$\delta \times 10^{15}$ (lines/m <sup>2</sup> )	ε x 10 <sup>-3</sup>
	26. 58 3	110	3.35 1	0.29	29.4 48	1.15 3	5. 34 8
	31. 81 3	103	2.81 1	0.30	28.4 68	1.23 4	4. 64 0
es	33. 76 8	101 *	2.65 2	0.33 4	25.9 92	1.48 0	4. 79 6
Samples CuS	37. 81 6	111	2.37 7	0.27 9	31.3 81	1.01 5	3. 56 0
	48. 13 0	110	1.88 9	0.29 0	31.3 84	1.01 5	2. 82 9
	51. 58 2	211	1.77 0	0.30	30.7 43	1.05 8	2. 70 7
	52. 79 7	108	1.73 3	0.46 9	19.7 50	2.56 4	4. 12 3
	54. 62 7	220	1.67 9	0.37	24.9 19	1.61 0	3. 16 6
		Ave	erage		27.7 61	1.39	3. 89 6
Ti: 2%	26. 61 3	110 *	3.34 7	0.27 3	31.2 17	1.02 6	5. 03 9
	31. 84 1	103	2.80 8	0.29 8	28.9 85	1.19 0	4. 55 3
	33. 79 8	101	2.65 0	0.32	26.8 69	1.38 5	4. 63 5
	37. 84 5	111	2.37 5	0.27	32.1 89	0.96 5	3. 46 8
	48. 16	110	1.88	0.27	33.2 73	0.90	2. 66

	0						7
							′
	51.	211					2.
	61	*	1.76	0.29	31.5	1.00	63
	2		9	2	44	5	6
	52.	108	4 70	0.46	20.4	2.47	4.
	82 3		1.73	0.46 1	20.1 11	2.47	04 7
	54.	220	2	1	11	2	2.
	65	*	1.67	0.35	26.5	1.41	96
	2		8	1	79	6	7
		Ave	erage		28.8	1.29	3.
					46	5	75
	2.6	440	1				2
Ti: 6%	26. 69	110 *	3.33	0.25	34.1	0.85	4. 59
076	1		7	0.23	60	7	2
	31.	103			- 55	,	4.
	91		2.80	0.29	29.1	1.17	51
	9		2	6	41	8	8
	33.	101					4.
	87	*	2.64	0.32	26.5	1.42	68
	1	111	4	7	25	1	6
	37. 92	111 *	2.37	0.27	31.9	0.98	3. 49
	3		1	5	07	2	2
	48.	110			0.		2.
	23		1.88	0.28	32.5	0.94	72
	8		5	0	13	6	5
	51.	211					2.
	68	*	1.76	0.25	36.8	0.73	25
	3 52.	108	7	0	23	8	6 3.
	90	100	1.72	0.37	24.9	1.60	25
	1		9	1	98	0	1
	54.	220					2.
	73	*	1.67	0.33	28.1	1.26	79
	7		6	2	37	3	9
		Ave	erage		30.5	1.12	3.
					25	3	54 0
Ti:	26.	110					5.
10%	68	*	3.33	0.28	29.9	1.11	23
	4		8	4	89	2	1
	31.	103					4.
	91		2.80	0.28	29.8	1.12	40
	0	461	2	9	71	1	9
	33.	101 *	2.64	0.27	22.0	0.07	3.
	87 2	Î	2.64 4	0.27 0	32.0 89	0.97 1	87 3
	37.	111	_	U	03	1	3.
	91	*	2.37	0.26	32.8	0.92	39
	4		1	7	57	6	2

48.	110					2.
23		1.88	0.28	31.9	0.97	77
1		5	4	73	8	1
51.	211					2.
68	*	1.76	0.23	38.5	0.67	15
3		7	9	76	2	3
52.	108					2.
90		1.72	0.33	27.7	1.29	92
2		9	3	97	4	4
54.	220					2.
71	*	1.67	0.32	28.4	1.23	76
6		6	8	84	3	6
	Ave	erage	31.4	1.03	3.	
				55	8	44
						0

## 4. SEM Analyses

Figure 4.12 shows the SEM images of undoped and titanium-doped copper (II) sulfide thin films deposited at different concentration of titanium ions. The SEM images revealed agglomerated particles of different sizes and shapes. The undoped copper (II) sulfide film contained spherical-like particle sizes that are less densely packed. The surface morphology of the film deposited at titanium concentration of 2 % showed the formation of larger spherical-like particles that are not well distributed on the substrate when compared to the undoped copper (II) sulfide film. Increasing the doping concentration to 6 % leads to the increase in the number of clusters and agglomerated nanoparticles. At further increase in doping concentration (10 %), the particle sizes of the film decreased, and the grains became unevenly distributed on the substrate. From the results, however, particles of the films are of unequal distribution, which suggest formation polycrystalline thin films of copper sulfide and titanium-doped copper (II) sulfide thin films.

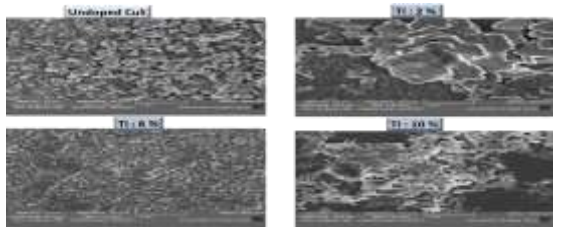


Figure 12: SEM images of undoped and titaniumdoped copper (II) sulfide thin films at different percentages of titanium ion

## 5. EDS Analyses

Figure 4.13 (a) and (b) showcase the elemental composition of the undoped copper (II) sulfide and titanium-doped copper sulfide thin films, respectively. Fig. 4.13 (a) confirms the presence of the anticipated elements (Cu and S) in the deposited film, but with some impurity atoms. Also, Fig. 4.13 (b) confirms the presence of the anticipated elements (Cu, S, and Ti) in the deposited film, but with some impurity atoms. The presence of impurity atoms (silicon, calcium, and oxygen), was as a result of the composition of the glass substrate.

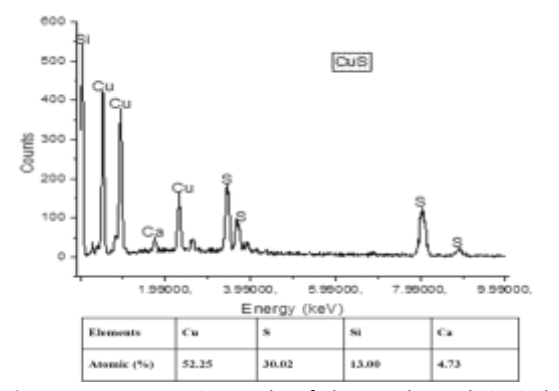


Figure 13 (a): EDS graph of the undoped CuS thin film

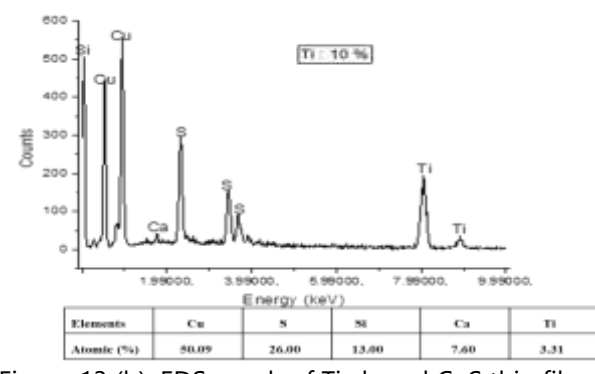


Figure 13 (b): EDS graph of Ti-doped CuS thin film

## **6. Electrical Analyses**

Electrical properties of titanium-doped copper (II) sulfide thin films synthesized at different titanium ion concentration are shown in Table 4.4. The result revealed a variation in the electrical properties due to the doping of copper (II) sulfide with titanium ion. Electrical resistivity value of  $58.89 \times (10)^{-5}$ 

 $\Omega$ m and conductivity of  $1.70 \times [(10)]^3$  (S/m) were obtained for the undoped CuS thin film. Close observation showed that immediately titanium ion introduced, the films' resistivity decreased to 11.37×[10]\(^(-5)  $(\Omega m)$ , decreased further to  $7.68 \times [10]^{-5}$  $\Omega$ m, as percentage doping was increased from 2 % to 6 %. But at peak value of 10 %, the resistivity value slightly increased to  $9.34 \times [10]^{-5}$   $\Omega$ m. While the films' resistivty was decreasing, the electrical conductivity of the films was found to have increased from  $8.70 \times [10]^3$  S/m to  $13.02 \times [10]^3$ S/m, which later decreased to 10.71×[10]<sup>^3</sup> S/m as the resistivity value increased. The decrease in electrical conductivity could be attributed to the increase in the thickness of the deposited thin films, due to the increase in titanium ion concentration. The graph of electrical resistivity and conductivity against percentage of titanium ion is shown in Figure 4.14.

Table 4: Electrical properties of titanium-doped copper (II) sulfide thin films deposited at different titanium doping concentrations

thaniam doping concentrations									
Dopant Conc.	$V \times 10^{-3}$ (volts)	$I \times 10^{-5}$ (amps)	Thickness (nm)	$\rho \times 10^{-5}$ $(\Omega m)$	$\sigma_e \times 10^3$ (S/m)				
CuS	38.33	3.22	109.16	58.89	1.70				
Ti: 2 %	3.77	1.70	113.17	11.37	8.70				
Ti: 6 %	7.26	5.19	121.11	7.68	13.02				
Ti: 10 %	10.18	6.51	131.79	9.34	10.71				

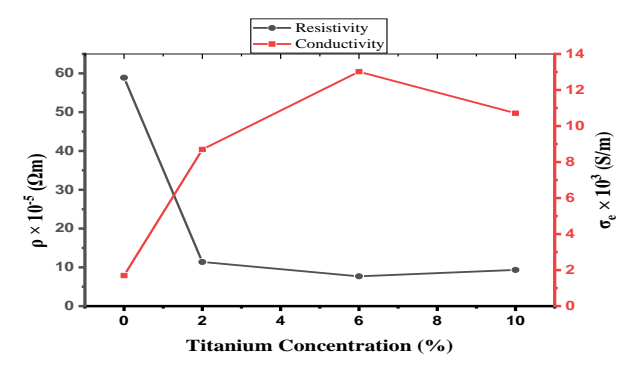


Figure 14: Variation of electrical resistivity and conductivity with percentage of titanium ion.

## 7. Magnetic analyses of the deposited thin films

The magnetic properties of Ti-doped copper (II) sulfide thin films were analyzed using a vibrating sample magnetometer (VSM) at room temperature to study the impact of Ti ion substitution within a range of -60000 to 60000 (Oe). The findings are shown in Fig. 4.15. The magnetic hysteresis loops of the samples did not saturate, even when exposed to the highest measured field, showing their antiferromagnetic properties. Increasing Ti doping from 2% to 6% resulted in an increase in maximum magnetization (Mmax) from -0.00057 to 0.00048 emu/g. The increase in magnetization intensity of these films could be because of the changes in cation and anion valence during annealing and transformation of the crystalline structure caused by Ti doping. The highest magnetization rose as the titanium ion content increased. Also, the films showed low coercivity (Hc), and the results showed that higher permeability was associated with lower coercivity.

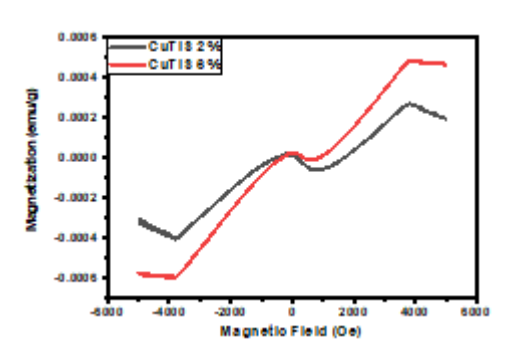


Figure 15: M – H Curves for Ti-doped CuS films deposited at 2 % and 6 % Ti conc.

## IV. CONCLUSION

With the use of electrodeposition technique, copper (II) sulfide thin film and Ti-doped copper (II) sulfide thin films have been successfully deposited onto conducting glass substrate (FTO), at room temperature. Thickness of the films were obtained using a profilometer, and the values obtained revealed that the films' thickness increased with increase in Ti doping concentration. Optical, structural, morphological, elemental, electrical, and magnetic properties of the electrodeposited films have been investigated, and observation showed that properties of the films were affected by the

doping percentage. Optical absorbance values of the films were found to have increased as percentage of titanium was increased, while transmittance values of the films were found to have decreased as the dopant concentration was increased. Also, from the results obtained, Ti-doped CuS films recorded low reflection compared to the undoped CuS films. This could be attributed to the high absorbance nature of the films, caused by the thickness, which increased as the titanium percentage concentration was increased. Other optical properties such as extinction coefficient, refractive index, optical conductivity real and imaginary dielectric constants, and energy band gap were estimated using established expressions from our reviewed literatures. The energy bandgap varied from 2.40 eV to 2.60 eV, as the doping concentration was varied. EDS spectra of the films revealed atomic percentages of elements present in the films. The films crystallize well in the hexagonal structure with preferential orientation of the crystallites along the (103) plane. The average crystal sizes range from 27.761nm to 31.455 nm. The results obtained showed that, with the increase in dopant percentage, crystallite size of the films increased, while dislocation density and microstrain decreased. The SEM images revealed agglomerated particles of different sizes and shapes. However, the film deposited at 6 % Ti doping has a better and homogeneous surface. Electrical conductivity and resistivity of the films varied with respect to the percentage doping. As conductivity decreased, resistivity increased. From the VSM analyses, the films exhibited clear hysteresis loops at room temperature, and there was no observed magnetic saturation, even at higher applied magnetic fields, which confirmed the antiferromagnetic nature of these films.

## Acknowledgement

This research was supported by TETFUND, with the reference number TETF/DR&D-CE/NRF 2021/SETI/ICT/00034/01

## **REFERENCES**

- Nuemann, T.; Feldmann, S.; Moser, P.; Delhomme, A.; Zerhoch, J.; Goor, T.; Wang, S.; Dyksik, M.; Winkler, T.; Finley, J. J.; Plochocka, P.; Brandt, M. S., Faugeras, C., Stier, A. V., and Deschler, F. Manganese doping for enhanced magnetic brightening and circular polarization control of dark excitons in paramagnetic layered hybrid metal-halide perovskites. Nature Commun. 12 (2021):3489; 1-8. https://doi.org/10.1038/s41467-021-23602-1.
- Gupta, A., Zhang, R., Kumar, P., Kumar, V., and Kumar, A. Nano-structured dilute magnetic semiconductors for efficient spintronics at room temperature. Magnetochemistry 6 (2020):15; 1-22.
  - https://doi:10.3390/magnetochemistry6010015.
- Nemsak, N., Gehlmann, M., Lin, C. S., Schlueter, C., Mlynczak, E., Lee, T., Plucinski, L., Ebert, H., Marco, I. D., Minar, J., Schneider, C. M., and Fadley, C. S. Elemental-and momentum-resolved electronic structure of the dilute magnetic semiconductor manganese doped gallium arsenide. Nature Commun. 9(2018):3306; 1-8. https://doi.org/10.1038/s41467-018-05823-z.
- Dietl, T. A ten-year perspective on dilute magnetic semiconductors and oxides. Nature Material 9(2010); 965 – 974. https://doi:10.1038/NMAT2898.
- Zhang, Z. H., Wang, X., Xu, J. B., Muller, S., Ronning, C., and Li, Q. Evidence of intrinsic ferromagnetism in individual dilute magnetic semiconducting nanostructures. Nature Nanotech 4 (2009); 523-527. https://doi.org/10.1038/nnano.2009.181.
- Liu, W., Zhang, H., Jin-an Shi, Wang, Z., Song, C., Wang, X., Siyuan Lu, Zhou, X., Lin Gu, Louzguine-Luzgin, D. V., Chen, M., Yao, K., and Na Chen. A room-temperature magnetic semiconductor from a ferromagnetic metallic glass. Nature Commun. 7(2016); 1-6. https://doi:10.1038/ncomms13497.
- 7. Wolf, S. A., Awschalom, D. D., Buhrman, R. A., Daughton, J. M., von Molnar, S., Roukes, M. L., Chtchelkanova, A. Y., and Treger, D. M. (2001). Spintronics: A spin-based electronics vision for

- the future. Science 294(2001):5546; 1488-95. https://doi:10.1126/science.1065389
- 8. Kaushik, H. S., Sharma, A., and Sharma, M. Dilute magnetic semiconductor: A review of theoretical status. IJIEASR 3(2014):1; 5 10.
- Murtaza, G., Ahmad, R., Rashid, M. S., Hassan, M., Hussnain, A., Khan, M. A., Ehsan ul Haq, M., Shafique, M. A., and Riaz, S. (2014). Structural and magnetic studies on Zr doped ZnO diluted magnetic semiconductors. Current Applied Physics 14(2014); 176 – 181.
- Philip, J., Punnoose, A., Kim, B. I., Reddy, K. M., Layne, S., Holmes, J. O., Satpati, B., LeClair, P. R., Santos, T. S., and Moodera, J. S. Carriercontrolled ferromagnetism in transparent oxide semiconductors. Nature Mater 5(2006); 298-304. https://doi.org/10.1038/nmat1613.
- Thanikaikarasan, S., Mahalingam, T., Kathalingam, A., Moon, H., and Kim, Y. D. (2010). Characterization of electrodeposited copper sulphide thin films. J. New Mat. Electrochem. Systems 13(2010); 29 – 33.
- Mohammed, K. A., Ahmed, S. M., and Mohammed, R. Y. (2020). Investigation of structure, optical, and electrical properties of CuS thin films by CBD technique. Crystals, 10(2020):684; 1-22. https://doi:10.3390/cryst10080684.
- 13. Sangamesha, M. A., Pushapalatha, K., Shekar, and G. L. Effect of concentration on structural and optical properties of CuS thin films. IJRET 2(2013):11; 227 234.
- Offiah, S. U., Ugwoke, P. E., Ekwealor, A. B. C., Ezugwu, S. C., Osuji, R. U., and Ezema, F. I. (2012). Structural and spectral analysis of chemical bath deposited copper sulphide thin films for energy conversion. Digest Journal of Nanomaterials and Biostructures 7(2012):1; 165 173.
- Nho, P. V., Ngain, P. H., Tien, N. Q., and Viet, H.
   Preparation and characterization of low resistivity CuS films using sparay pyrolysis. Chalcogenide Letters 9(2012):10; 397 – 402.
- Podder, J., Kobayashi, R. and Ichimura, M. Photochemical deposition of CuxS thin films from aqueous solutions. Thin Films, 472(2005); 71-75. https://doi:10.1016/j.tsf.2004.06.137.

- 17. Kassim, A., Min, H. S., Haron, M. J., and Nagalingam, S. Preparation of thin films of copper sulphide by chemical bath deposition. Int. J. of Pharm. & Life Sci. (IJPLS), 2(2011):11; 1190-1194.
- 18. Baki, N. A., Kamil, A. A, Jabbar, M. S., Rahman, H. Z. A. A. Deposition of CuS, ZnS, and their stacked layers thin films by chemical spray pyrolysis technique. Int. Sci. (Lahore) 30(2018): 2; 259-266.
- 19. Meshram, R. S. and Thombre, R. M. Structural and morphological properties of CuS thin films prepared by spray pyrolysis technique. JETIR 28. Jeroh, D. M., Ekpunobi, A. J., and Okoli, D. N. 8(2021):12; 46-49. The optical properties of europium-doped zinc
- 20. Martinson, A. B. F., Elam, J. W., and Pellin, M. J. Atomic layer deposition of Cu2S for future application in photovoltaics. Applied Physics Letters 94(2009):12; 123107. https://doi:10.1063/1.3094131.
- 21. Wu, C., Jen-Bin Shi, Chih-Jung Chen, Yu-Cheng Chen, Ya-Ting Lin, Po-Feng Wu, and Sung-Yen Wei. Synthesis and optical properties of CuS nanowires fabricated by electrodeposition with anodic alumina membrane. Materials Letters 62(2008); 1074-1077. https://10.1016/j.matlet.2007.07.046.
- 22. Najm, I. S., Mahmood, S., Kadhim, A. A., and Alwahib, A. A. Investigation of the CuS thin film prepared by pulsed laser deposition. Materials Today: Proceedings 42 (2021); 2609-2615. https://doi:10.1016/j.matpr.2020.12.589.
- 23. Guangwei, S., Lixuan, M., and Wensheng, S. Electrodeposition of one-dimensional nanostructures. Recent Patents on Nanotechnolgy, 3(2009):3; 182 191. https://doi:10.2174/187221009789177777.
- 24. Mahalingam, T. and Thanikaikarasan, S. Influence of solution pH in electrodeposited iron diselenide thin films. J. Alloys and Compounds, 511(2012); 11 122.
- 25. Yıldırım, A, K. and Altıokka, B. An investigation of effects of bath temperature on CdO films prepared by electrodeposition Appl Nanosci. 7(2017); 513–518. https://doi.org/10.1007/s13204-017-0591-x.
- 26. Dharmadasa, I. M., Madugu, M. L., Olusola, O. I., Echendu, O. K., Fauzi, F., Diso, D. G., Weerasinghe, A. R., Druffel, T., Dharmadasa, R.,

- Lavery, B., Jasinski, J. B., Krentsel, T. A. and Sumanasekera, G. (2017). Electroplating of CdTe thin films from cadmium sulphate precursor and comparison of layers grown by 3-electrode and 2-electrode systems. Coatings 7 (2017), 1 17. https://doi:10.3390/coatings7020017.
- 27. Song, J., Li, S. S., Yoon, S., Kim, W. K., Kim, J., Chen, J., Craciun, V., Anderson, T.J., Crisalle, O. D. and Ren, F. Growth and Characterization of CdZnS Thin Film Buffer Layers by Chemical Bath Deposition, 31st IEEE Photovoltaic Specialists Conference (2005), 449 451.
- Jeroh, D. M., Ekpunobi, A. J., and Okoli, D. N. The optical properties of europium-doped zinc selenide films. Journal of Nano-and electronic Physics 12(2020): 5, 05006. https://doi:10.21272/jnep.12(5).05006.
- 29. Okoli, N. L., Ezenwaka1, L. N., Okereke, N. A., Ezenwa, I. A., and Nwori, N. A. Investigation of optical, structural, morphological and electrical properties of electrodeposited cobalt doped copper selenide (Cu1-xCoxSe) thin films. Trends In Sciences 19(2022):16, 5686. https://doi.org/10.48048/tis.2022.5686.
- 1074-1077. 30. Okoli, D. N. Optical properties of chemical bath deposited magnesium sulphide thin films.

  A. A., and Chemistry and Materials Research 7(2015):2; uS thin film 61-68.
  - 31. Babatunde, R. A. and Bolanle, Y. I. Effect of annealing on optical and electrical properties of magnesium sulphide (MgS) thin film grown by chemical bath deposition method. International Journal of Scientific Research in Physics and Applied Sciences 8(2020):3; 60 64.
  - 191. 32. Sagadevana, S. and Das, I. Chemical bath deposition (CBD) of zinc selenide (ZnSe) thin films and characterization. Australian Journal of Mechanical Engineering, 15(2016):3; 222 227. https://doi.org/10.1080/14484846.2016.126434 7.
    - 33. Bekkari, R., Jaber, B., Labrim, H., Quafi, M., Zayyoun, N. and Laahab, L. Effect of solvents and stabilizer molar ratio on the growth orientation of sol gel derived ZnO thin films. International Journal of Photoenergy 2019(2019):1a; 1 7. https://doi.org/10.1155/2019/3164043.

- 34. Ongwen, N. O., Oduor, A. O. and Ayieta, E. O. Effect of concentration of reactants on the optical properties of iron – doped cadmium stannate thin films deposited by spray pyrolysis. American Journal of Materials Science, 9(2019):1: 1-7.
- 35. Axelevitch, A., Gorenstein, B., and Golan, G. Instigation of optical transmission in thin films. Procedia 32(2012): Physics 1 https://doi:10.1016/j.phpro.2012.03.510.
- 36. Mushtaq, S., Ismail, B., Raheel, M. and Zeb, A. Nickel Antimony Sulphide Thin Films for Solar Cell Application: Study of Optical Constants. Natural Science, 8(2019): https://doi:10.4236/NS.2016.82004.
- 37. Kariper, I. A. The production of UV absorber amorphous cerium sulfide thin film. Materials Research 20(2017):5; 1345-1349. http://dx.doi.org/10.1590/1980-5373-MR-2016-0917.
- 38. Guneri, E. The role of Au doping on the structural and optical properties of Cu2O films. Journal of Nano Research, 58(2019); 49 - 67. https://doi:10.4028/www.scientific.net/JNanoR.5 8.4.
- 39. Sharma, P. and Katyal, S. C. Determination of optical parameters of a-(As2Se)90Ge10 thin film. Journal of Physics D: Applied Physics, 40(2007):7; 2115 2120. https://doi:10.1088/0022-3727/40/7/038.
- 40. Akpu, N. I., Sylvanus, C. A., Nwaokorongwu, E. C., Imosobomeh, L. I., Okechukwu, E. O., Ugwu, L. U., and Ekpunobi, A. J. Modulation of the physical properties of spray-deposited cobalt selenide nanofilm via yttrium doping for photovoltaic purposes. J. Mater. Environ. Sci. 14(2023):11; 1230-1244. http://www.jmaterenvironsci.com
- Effect of doping concentration on the structural and optical properties of pure and tin doped zinc oxide thin films by nebulizer spray pyrolysis (NSP) technique. Superlattices and Microstructures, 52(2012):3; 500-513. https://doi:10.1016/j.spmi.2012.05.016
- 42. Hennayaka, H. M. M. N. and Lee, H. S. Structural and optical properties of ZnS thin film grown by pulsed electrodeposition. Thin Solid Films

- (2013):32567. http://dx.doi.org/10.1016/j.tsf.2013.09.011
- 43. Jafari-Rad, A. and Kafashan, H. Preparation and characterization of electrochemically deposited nanostructured Ti-doped ZnS thin films. Ceramics International, 45(2019): 21413 -21422.
  - https://doi.org/10.1016/j.ceramint.2019.07.130
- 13. 44. Sharma, L. K., Kar, M., Choubey, R. K., and Mukherjee, S. Low field magnetic interactions in the transition metals doped CuS quantum dots. Chemical Physics Letters 780(2021): 138902. https://doi.org/10.1016/j.cplett.2021.138902
- 33-40. 45. Guneri, E. and Kariper, A. Optical properties of amorphous CuS thin films deposited chemically at different pH values. Journal of Alloys and 516(2012): Compounds 20 26. https://doi:10.1016/j.jallcom.2011.11.054
  - 46. Awada, C., Whyte, G. M., Offor, P. O., Whyte, F. U., Kanoun, M. B., Goumri-Said, S., Alshoaibi, A., Ekwealor, A. B. C., Maaza, M. and Ezema, F. I. Synthesis and Studies of Electrodeposited Yttrium Arsenic Selenide Nanofilms for Opto-Electonic Applications. Nanomaterials, 10(2020):1557.
    - https://doi:10.3390/nano10081557
  - 47. Jafari-Rad, A. and Kafashan, H. Preparation and characterization of electrochemically deposited nanostructured Ti-doped ZnS thin films. Ceramics International, 45(2019): 21413
    - https://doi.org/10.1016/j.ceramint.2019.07.130
  - 48. Okechukwu, E. O. and Okoli, D. N. Optical and structural properties of electrodeposited CdS/ZnS compound thin films and their possible applications. Journal of Materials Sciences and Applications 1(2015):6; 282-291. http://www.aascit.org/journal/jmsa
- 41. Mariappan, R., Ponnuswamy, V., and Suresh, P. 49. Tezel, F. M. and Kariper, I. A. (2019). Effect of pH on the structural and optical properties of polycrystalline ZnSe thin films produced by CBD method. International Journal of Modern **Physics** 1950024, 1 13. 33(5), http://dx.doi.org/10.1590/1980-5373-MR-2017-
  - 50. [Awada, C., Whyte, G. M., Offor, P. O., Whyte, F. U., Kanoun, M. B., Goumri-Said, S., Alshoaibi, A., Ekwealor, A. B. C., Maaza, M. and Ezema, F. I.

Emmanuel O. Okechukwu. International Journal of Science, Engineering and Technology 2025, 13:3

Synthesis and Studies of Electrodeposited Yttrium Arsenic Selenide Nanofilms for Opto-Electonic Applications. Nanomaterials, 10(2020):1557. https://doi:10.3390/nano10081557